A Cost-effective Photovoltaic Architecture with Dual Quantum Tunneling in a Monolithic Perovskite/Si Tandem Device

Z.Q. Ma*, K.J.Wu, Z.X.Lan, Y.L.Wang, F.Xu and L.Zhao

SolarE PV joint laboratory, Department of Physics, Shanghai University, Shanghai (China)

Abstract

A 2-terminal monolithic tandem photovoltaic architecture was conceptually constructed with both organic-inorganic metal halide perovskite upper cell and asymmetric Si-based heterojunction dual carrier's tunneling bottom cell. The interconnection layer of the cells was indium tin oxide (ITO) film of about 80 nm formed by r.f magnetron sputtering deposition of hole selected ultra-thin passivating contact a-SiO_x(In) layer on silicon substrate. At rear side of the Si wafer a wet nitric acid oxidized silicon layer SiO_x (<1.6 nm) and subsequently d.c magnetron sputtered TiN_y coupling layer of SiO_x/TiN_y acted as electron passivated contact. Thus, the quantum tunneling of hole and electron through two kinds of silicon oxides was realized. The analyses of the graded distribution of In, Si and O elements in the interfacial region of ITO/n-Si and amorphous lattice morphology of the ultrathin a-SiO_x(In) layer were gained through the characterizations of X-ray photoemission spectroscopy and high-resolution transmission electron microscope. The intrinsic and p-type conductance of ultrathin SiO_x(In) layer was modeled by molecular dynamics and density function theory. The good photovoltaic feature of the devices has been obtained by current-voltage measurement under AM 1.5G illumination, and its optimized PV character has been simulated by AFORS-HET program. Finally, the Si-based bottom cell was cohered by an efficient n-i-p perovskite cell as a monolithic tandem PV device. The power conversion efficiency of the tandem device has been numerically predicted to be more than 29 % by combining the experimental and simulation data, under the optimized parameters of J_{sc}, V_{oc} and pFF.

Keywords: Tandem cells, photoelectric conversion, SQIS structure, quantum dual tunneling

1. Introduction

Nowadays, the efforts strive to amalgamate the exceptional performance of those organic-inorganic metal halide perovskite solar cells (PSCs) with market-established photovoltaic (PV) technologies such as crystalline silicon (c-Si) solar cells in the form of perovskite/silicon tandems has been mentioned to the agenda of science and technology development (Chen et al. 2019; Jošt et al. 2018; Mazzarella et al. 2019; Nogay et al. 2019; Sahli et al. 2018). Such two-terminal tandems hold the promise to enable a very high-performance PV technology, surpassing single-junction efficiency limits, with high market relevance. Scientifically, in addition to desirable properties such as high absorption coefficient, low Urbach energy, and long charge carrier's diffusion lengths of the perovskite materials, especially, the bandgap can be easily tuned by varying their composition of I/Br ratio. Alongside these properties, the availability of various fabrication techniques that are compatible with deposition on textured c-Si substrates, has been vital toward the development of efficient perovskite/silicon tandem solar cells (Al-Ashouri et al. 2020; Jošt et al. 2020; Roß et al. 2021; Wang et al. 2021). However, the critical challenges that require sustained research efforts are device stability of PSCs architecture, cost-efficient massive-scale processing, and the fulfillment of the perovskite/silicon tandems to yield PCEs well beyond 30%. Fortunately, for the single-junction PSCs, the n-i-p architecture has been most successful to date in terms of device performance, thanks to defect and interface passivation, from which the perovskite-Si tandem research become more beneficial (Liu et al. 2020; Jeong et al. 2021a, 2021b; Zheng et al. 2020). Thus, an effective tandem scheme is present for the n-i-p perovskite / c-Si solar cell and its power conversion efficiency (PCE) has been mainly investigated so far.

In addition, metal halide perovskite solar cells (PSCs) have become the most promising new-generation solar cell technology. To date, perovskites also represent the only polycrystalline thin-film absorber technology that has enabled > 25.5 % efficiency for wide-bandgap solar cells (NREL 2021), making wide-bandgap PSCs uniquely positioned to enable high efficiency and low-cost tandem solar cell technologies by coupling wide bandgap perovskites with low-bandgap absorbers, such as crystalline silicon, CIGS or itself with lower band gaps (Kim et al. 2019; Mazzarella et al. 2019; Nogay et al. 2019; Sahli et al. 2018; Yang et al. 2019).

On the other side, for single-junction solar cells of monocrystalline silicon based material, the ultimate PCE is governed by the Shockley–Queisser theoretical limit (29.43%) (Shockley and Queisser, 1961). The primary

doi:10.18086/swc.2021.06.02 Available at http://proceedings.ises.org

energy loss of a single-junction solar cell includes the unabsorbed long-wavelength photons and thermalization of high-energy photon-generated carriers (Nelson et al. 2013). Nevertheless, the appropriate overlying design may plenarily harness solar energy converting electric power through wide spectroscopic absorption of sun's light, i.e., high-energy photons are absorbed by the upper wide-bandgap subcell, and lower energy photons are absorbed by the bottom narrow-bandgap subcell (Eperon et al. 2017). Of course, the matching of short-circuit current density (mA/cm^2) between top and bottom cells should be satisfied for any materials.

Furthermore, in accordance with the PV enhancement principles mentioned above, a realistic option has been proposed for the tandem scheme. As we know, high photoelectric conversion efficiency of crystalline silicon photovoltaic (PV) devices, so far, besides silicon heterojunction (SHJ) and tunneling oxide passivation contact (TOPCon's) types with heterojunction or homojunction, respectively, other types have been developed with improved technologies in time line. But, top cells in this tandem schematic require planar surfaces for fabrication, e.g., due to spin-coated layers, thus need to be in n-i-p configuration. Currently, silicon-based heterojunction solar cells provide more flexibility in this regard and can be used in either polarity. Besides, typical SHJ cells already feature a front transparent conductive oxide (TCO) layer that can serve as the perovskite's bottom contact similarly as in single-junction perovskite solar cells, allowing for relatively simple process integration. Thus, in the past, much greater efforts are devoted to developing tandem cells based on SHJ solar cells. Additionally, the advantage of Si heterojunction cells lies in their very high efficiency, brought about by a very high V_{oc} of 740 mV and a certified efficiency of 26.6% (Yoshikawa et al. 2017). However, this device is fabricated with interdigitated back contacts, not suitable for 2T applications. On the other side, it is difficult to assemble a 2T tandem PV device through perovskite to Si-based TOPCon's cell, in spite of its high PCE.

Recently, we cultivated a simplified process to fabricate a dual tunneling Si-based PV device with indium tin oxide (ITO)/a-SiO_x(In) and SiO_x/TiN_x passivation contact layers for either hole and electron selectivity, respectively (Gao et al. 2017; Song et al. 2018; Wu et al. 2020). On the other hand, its optical and electronic structures on the front surface of the device were suitable for the interconnection to a metal halide perovskite device with a wide-bandgap as top one. Therefore, its potential PV feature could be expectant.

2. Monolithic tandem photovoltaic scheme

2.1 Preparation of SQIS device

2.1.1 Front configuration of SQIS device

In our experiments, the ITO thin films in the range of 80 -120 nm, acting as TCO functional layers possessing idiographic optical and electronic traits for their high transmission in visible region (> 88%) and quite low resistivity (< 0.2 mΩ·cm), were deposited on chemical polished solar grade n-type CZ silicon (100) wafers (ρ~1.5 Ω·cm) and glass-substrates (designated area: 2×2 cm^2) by radio frequency (r.f) magnetron sputtering, respectively. The source material was ceramic target of mixing 10 wt. % SnO_2 and 90 wt. % In_2O_3. Before transferring the chamber, the glass-substrates were systematically cleaned in acetone, alcohol, and deionized water for 10 min., and n-Si wafers were cleaned by RCA treatment and immersed in 5 % HF solution for 100 seconds to get rid of native oxide. Prior to each deposition run, the sputtering chamber was evacuated to below 3×10^{-4} Pa. Simultaneously, Ar gas flow of 40 sccm held the gas pressure in the plasma fixed at 1.0 Pa during sputtering to maintain the Si substrate at room temperature. Then, Ag and Al metals were thermally evaporated on the front and rear side of n-Si substrate and subsequently medium temperature alloyed to form electrodes. Thus, a simplified crystalline silicon based optoelectric device was yielded with asymmetric structure and heterojunction style.

In order to gain the microstructure (chemical configuration and physical phase) of the intermediate zone of ITO-Si, the electronic states, and elemental ratio profiling and chemical components of ITO/c-Si interface region was analyzed by X-ray photoemission spectroscopy (XPS) with depth etching. The result was shown in Fig.1a, in which an ultra-thin amorphous silicon oxide layer (a-SiO_x) including indium (In) was synthesized by a solid-phase reaction during the sputtered-induced ITO components absorbed on n-Si substrate to form Si-O or Si-O-In bonds, of which the atomistic configuration and interfacial density of state (DOS) was studied in our previous report by molecular dynamics (MD) and density function theory (DFT) calculation (Wan et al. 2017). The amorphous lattice morphology of the ultrathin a-SiO_x(In) layer and its rough thickness (< 2.0 nm)

was characterized by high-resolution transmission electron microscope (HR-TEM) as manifested in Fig.1b, in which the indium element was included in the ultrathin a-SiO_x(In) layer (1.4-1.6 nm) and acted as an accepted impurity. X-ray source used for XPS (Thermo fisher, Escalab 250Xi) analyses was Al Kα (~1486.6 eV), where the work function of ITO films in the scope of 4.90 – 5.06 eV was also evaluated by ultra-photoemission spectroscopy (UPS) excited through He I line (~21.22 eV) (Gao et al. 2017). The forward sputtering power dependent variation of O/Si ratio and silicon suboxide compositions at etching time of 960 s were shown in Fig.2. A mathematical deconvolution analysis has been carried out for the Si 2p states in Si_2O, SiO, Si_2O_3, SiO_2 as well as Si $2p_{3/2}$ or Si $2p_{1/2}$ components, depending on the typical binding energy values (Dreiner et al. 2001).

Accordingly, the delocalized electronic states at E_v + 0.3 eV and p-type conductivity near n-Si surface has been induced by the combination of indium (In) element with oxygen and silicon within the interfacial region of ITO film and n-Si substrate (Wan et al. 2017), supporting by numerical calculation of partial and total density of state (DOS) of a-SiO_x(In) layer and DFT as well. Thus, the transport modes of photo-generated hole through the a-SiO_x(In) layer by the ways of tunneling, assisted-tunneling, recombination or diffusion become possible in the present situation.

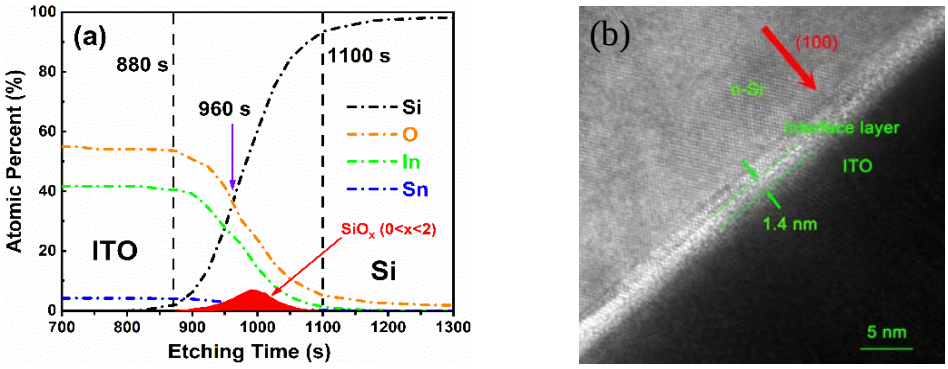

Fig.1 (a) Atomic percentage of elements in the ITO/n-Si interface region varied with etching time by XPS, including the In, Sn, O and Si elements, also SiO_x oxide; (b) Microscope of intermediate layer a-SiO_x(In) by HR-TEM.

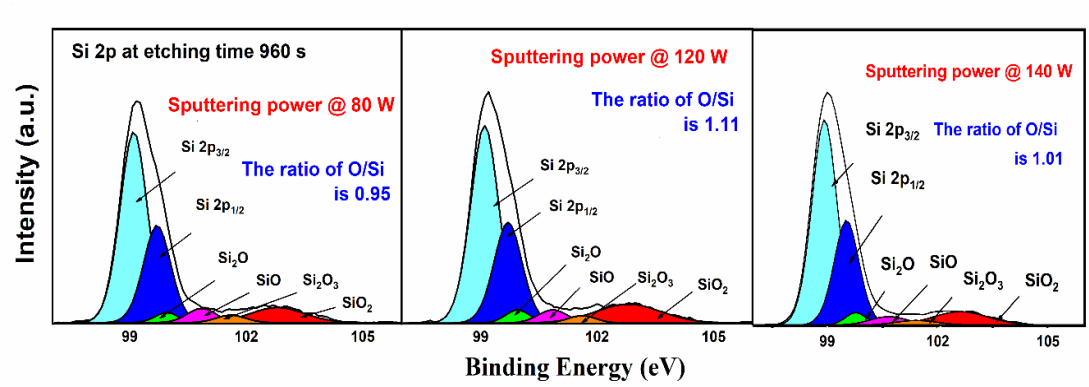

Fig.2 Detailed peak-peak fitting of Si 2p spectra at the etching time of 960s for 80, 120 and 140 W, and the relative proportion of O/Si in amorphous a-SiO_x(In) layer, respectively.

Subsequently, the typical thickness of 80 nm ITO film was deposited on Si substrate by varying sputtering power from 80 to 140 W. Then, Ag and Al metals were alloyed contact by vacuum thermal evaporation, respectively, as front and rear electrodes and the Ag/ITO/a-SiO_x/n-Si/Al device was constructed. Mobility of the ITO film was measured by a four-point probe Hall system (HL5500-PC). The characteristics on short-circuit current density (J_{sc}) to open-circuit voltage (V_{oc}) of ITO/a-SiO_x/n-Si heterojunction PV devices (Named as SQIS) were measured though one-sun's solar simulator system (Sciencetech, SS-150-A). By measuring the lifetime of minority carriers, it is possible to evaluate the effect of different surface treatment processing on surface passivation. Since the front and back surfaces of SQIS heterojunction solar cells were asymmetric, we used the same process to sputter ITO films on the front and back surfaces of silicon. The mode of minority carrier lifetime tester used in our laboratory was WT2000 of Semilab Co. The approach can be referred to

Gao's report in 2017.

Concerning on the photon-generated current associated with the carrier transport through the heterojunction of SQIS device, the obtained larger J_{sc} means that the main contribution arises from minority carrier (hole) near the inversion layer of n-Si absorber. However, the a-SiO_x(In) layer offers a high potential barrier prevent the carriers from the diffusion and shift moving to the end. Hence, a quantum tunneling is quoted to explain the transport behavior. For the electrons in n-Si side, although the effective interaction from both the built-in-potential in inversion layer and a little recombination through the interface states are present, the most of electron might transfer to the end as a negative charge accumulation. On the other hand, the hole induced by photon-excited and near the interface of n-Si side has to tunnel through the high barrier of SiO_x layer. Thus, the accumulation of holes on the opposite end, in virtue of the characteristic of ITO as double performances of semiconductor and quasi-metal, is the proof by the measurable V_{oc}. Basing on the above-mentioned picture, the schematic energy band diagram of ITO/SiO_x/n-Si, at short-circuit condition and under illumination case, is here shown in Fig.3 (a).

We are successful at last making an ideal opto-electric diode with PV characteristic, where the functions of passivation and tunneling are achieved at the same time. Actually, the implement has been done without any premeditation for the solution of our difficulty. The prototype concerning about ITO/a-SiO_x(In)/n-Si heterojunction photovoltaic device is simply fabricated by r.f magnetron sputtering of ITO on n-Si substrate at 150°C. Its J-V relationship is depicted in Fig. 3 (b), and the excellent rectifying characteristic (the saturation dark current density (J_0) can reach to 10^{-7} mA/cm^2) of the device is realized under dark J-V as well as the typical photovoltaic (PV) peculiarity of the device is obtained under AM 1.5G illumination (100 mW/cm^2). The power conversion efficiency (η) of the device is measured to be 11.47 %, together with open-circuit voltage (V_{oc}) of 0.49 V, short-circuit current density (J_{sc}) of 30.33 mA/cm^2 and fill factor (FF) of 77.15 %, without surface textured and extra back passivation treatment.

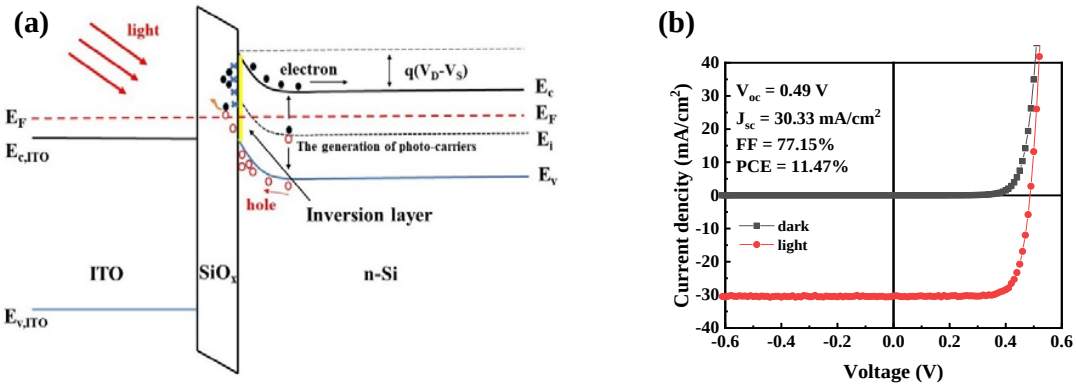

Fig.3 (a) Energy band of ITO / a-SiO_x (In) / n-Si device under one-sun illumination; (b) J-V curve of SQIS device under dark and light conditions, in addition the photovoltaic conversion parameters in AM 1.5 G illumination.

2.1.2 Rear passivation contact stacks of SQIS device (modified)

In this section, the extra passivation contact for SQIS device was replaced by SiO_x/TiN_y (where $0 < x < 2$; $0 < y < 1$) for Al-BSF. The cross-section of a modified SQIS was illustrated in Fig.4a, in which the ultrathin silicon oxide SiO_x (< 2 nm) was made through the formal nitric acid oxidation of silicon (NAOS) (Kobayashi et al. 2010) process and subsequently reactive magnetron sputtering method was used to lay titanium nitride film at room temperature. The detail experimental processing for fabricate ITO/a-SiO_x(In) composited film on n-Si by r.f magnetron sputtering can be inferred to our previous report (Du et al. 2015). The individual thickness of thin film materials in Fig.4a is also indicated. The quality of the rear SiO_x has been characterized by XPS as shown in Fig.4b, where a nearly stoichiometric SiO_2 is formed on monocrystalline n-Si substrate by the approach. Thus, it means that the chemical passivation of Si surface and the decline of interface state density of n-Si/SiO_x can be expected. When the numerical calculation is deployed to the optimized modified SQIS device, including surface textured and further rear passivation contact by SiO_x/TiN_y coupling layers, the performance of the PV device has been improved so much, and the detail results are given in the following subsections. Thus, the transport of photo-generated electron through the barrier of n-Si/SiO_2-TiN_y can be

interpreted by quantum tunneling besides other mechanisms.

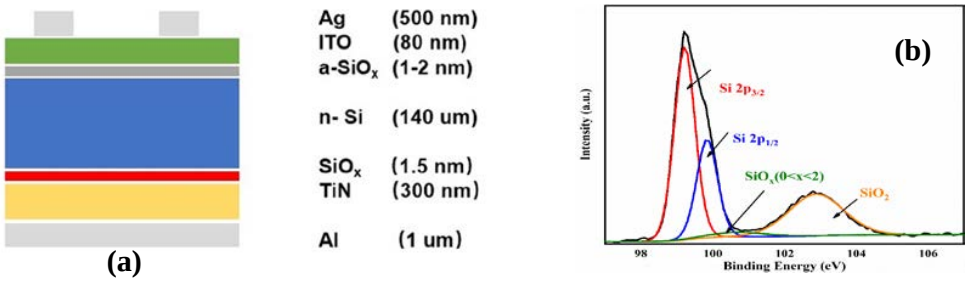

Fig.4 a) Schematic diagram of modified SQIS device; b) XPS of SiO_x/n-Si on rear surface.

2.1.3 Numerical simulation by AFORS-HET for both SQIS and modified-SQIS devices

Considering the structure of the device, the ITO/a-SiO_x(In)/n-Si/SiO_x/TiN_y is similar to that of the SHJ heterojunction device, which is often simulated by using AFORS-HET software of version 2.5. Therefore, we first simulate the photovoltaic performance of the SQIS, in which the material and interface of each layer was set as:

(1) Taking into account the orbital energy level induced by oxygen vacancies and indium element, we put dual effects with passivation and tunneling;

(2) The a-SiO_x (In) is divided into two layers for simulation, including the p-a-SiO_x (In) layer with negative charge center and the intrinsic passivation layer, i-a-SiO_x (In);

(3) The defect arisen from dangling bonds is set to be three types, namely Condce Tail, Valence Tail and Gauss, and the interface state density between i-a-SiO_x (In) and n-Si is 1.0 x 10^{11} cm^{-2} eV^{-1}, which refers to ref. (Wu et al. 2020);

(4) According to the literature, the band gap of the p-a-SiO_x (In) layer is set to be 2.06 eV, and the negative charge center concentration is 1 x 10^{17} cm^{-3};

(5) The ITO/p-a-SiO_x (In) interface is set to be Schottky contact, and both the ITO and TiN films are Ohm contact with the front and back electrodes, respectively.

Thus, the parameter settings of each layer and interface are listed in Table 1, while the other parameters are set to be the default values. On this basis, a SiO_x/TiN_y composite layer is arranged on the back of n-Si to simulate the photovoltaic performance of ITO/a-SiO_x(In)/n-Si/SiO_x/TiN_y device.

The photovoltaic performance of ITO/a-SiO_x(In)/n-Si and ITO/a-SiO_x(In)/n-Si/SiO_x/TiN_y heterojunction devices is simulated under the standard sunlight of AM 1.5G, and the result of its J-V curve is shown in Fig.5a. The open-circuit voltage of 0.58 V, short-circuit current density of 37.00 mA/cm^2, fill factor of 75.90 %, and conversion efficiency of 16.29 % are obtained, which are obviously better than that of experimental results of SQIS device (V_{oc} = 0.48 V, J_{sc} =2 9.93 mA/cm^2, FF = 6 9.90 %). As a SiO_x/TiN_y composite layer stacked on the back, the open-circuit voltage is increased by 0.13 V and finally obtains a high open-circuit voltage of 0.71 V, where the interface state density between n-Si and SiO_x layer is set to be 1.0 x 10^{11} $cm^{-2}eV^{-1}$. At the same time, there is a significant increase in each photovoltaic parameter, with a short-circuit current density of 40.05 mA/cm^2, a fill factor of 81.19 % and a conversion efficiency of 23.08 %.

It can be concluded that the optical and electrical gain from back passivation has extra contribution to the conversion efficiency of the device by 7.6 % and 18.3 %, respectively. We believe that the optical gain mainly depends on the absorption and reflection of near-infrared and mid-infrared light by the TiN_y film, because the silicon material is transparent loss to infrared light, accounting for about 42 % of the sun's light.

When simulated with AFORS-HET software, the applied electronic concentration of the composite SiO_x/TiN_y film material is set to be in the range of 10^{21}-10^{22} cm^{-3} for the best performance of the heterojunction device. Furthermore, the energy band structure of the SQIS device with multi-interface layer is shown in Fig.5b. It is found that the energy bending of the structure is about 0.92 eV, of which 0.75 eV is on the side of the ITO film

and 0.17 eV on the side of the ultrathin silicon oxide layer, so the larger bending can result in high open voltage. Referring to the previous report (Song et al. 2018), it is indicated that the energy band of the SQIS device was curved to 0.66 eV, while the energy band of the SQIS device with 5 nm n^+ - a-Si layer was bent to 0.87 eV, of which 0.73 eV was on the side of the ITO film and 0.14 eV on the side of the n^+ - a-Si film.

Tab.1: List of main simulation parameters of AFORS-HET for modified SQIS device

Parameters	p-a-SiO_x(In)	i-a-SiO_x(In)	SiO_x/TiN*	n-Si
Layer thickness (cm)	1.2×10^{-7}	2×10^{-8}	3×10^{-5}	1.5×10^{-2}
Dielectric constant	9	9	3.5	11.9
Electronic affinity (eV)	3.5	3.5	4.15	4.05
Mobility gap (eV)	2.06	2.06	3.40	1.12
Optical gap (eV)	2.06	2.06	3.40	1.12
Effective DOS in CB (cm^{-3})	2×10^{20}	2×10^{20}	6×10^{21}	2.84×10^{19}
Effective DOS in VB (cm^{-3})	2×10^{20}	2×10^{20}	1×10^{21}	2.68×10^{19}
Donor doping (cm^{-3})	-	-	10^{21}-10^{22}	2×10^{15}
Acceptor doping (cm^{-3})	1×10^{17}	-	-	-
Electron (hole) mobility (cm^2/Vs)	40(5)	40(5)	-	1321 (461)

Note: The thickness of the silicon oxide layer in the SiOx/TiN composite film is about 1.5 nm, and the TiN film is about 300 nm, hence having a high donor concentration.

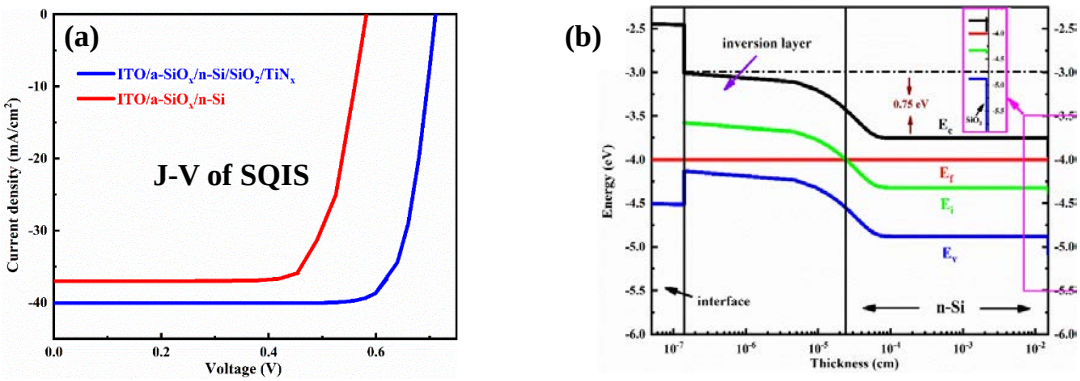

Fig.5 a) J-V curves of both ITO/a-SiOx/n-Si with and without extra SiO_2/TiNx; b) the variation of energy band vs thickness into modified-SQIS device, and special on rear passivation.

2.2 Selection of wide bandgap n-i-p perovskite PSCs as top cell

In the two-terminal monolithic tandem PV cells with 2 Shockley–Queisser limit junctions (2-SQJs), an optical bandgap of 1.75 eV is desirous for the top cell, when the bottom cell is c-Si absorber having the bandgap of 1.12 eV. Therefore, a well fabricated metal halide perovskite solar cell (PSCs) with a composition of $Cs_{0.12}MA_{0.05}FA_{0.83}Pb(I_{0.6}Br_{0.4})_3$ (Tan et al. 2018) has been selected as top cell in our optimized 2-SQJs PV system. Through incorporating 5% MA substituting partial Cs element in the previous composition of $Cs_{0.17}FA_{0.83}Pb(I_{0.6}Br_{0.4})_3$, so that its bandgap is still kept as same as a near-ideal bandgap of 1.74 eV (McMeekin et al. 2016). Furthermore, in the experiments, there is almost no hysteretic behaviors in short-circuit current density to open-circuit voltage (J-V) measurements, particularly, FF exceeds 80% and V_{oc} reaches to 1.25 V after the incorporation of a small amount of MA. Consequently, the stabilized PCE of 19.1% with dipolar MA cation in the device architecture of ITO/TiO_2–Cl/perovskite/Spiro-OMeTAD/Au is achieved on planar ITO substrate, where a thick perovskite layer of about 600 nm and an area of 1.1 cm^2 are validated for our modified c-Si SQIS case.

3. Prediction of conversion efficiency of the tandem system

The prediction of the PCE of the planar n-i-p perovskite/SQIS with stacked passivating contact and interconnection transport layers mainly obeys the following three principles:

1) For the entire stack device, silicon-based short circuit current density loses nearly half in that the EQE response by current matching of two cells;

2) Due to the decrease of short circuit current density and the recombination of interconnection layer, the open circuit voltage has a little lost;

3) Fill factor uses the comparison of the simulation results and the empirical formula.

3.1 Short-circuit current J_{sc}:

The relationship between short circuit current density and external quantum efficiency can be expressed as formula

$$J_{sc} = q\int F(\lambda)IQE(\lambda)[1-R(\lambda)]d\lambda = q\int F(\lambda)EQE(\lambda)d\lambda \qquad \text{(eq. 1)}$$

Where IQE (λ) [1-R (λ)] = EQE (λ), R (λ) is reflectivity, EQE (λ) and IQE (λ) are external quantum efficiency and internal quantum efficiency, respectively, F (λ) is the density of incident photon flow, q is the elemental charge. Metal halogen perovskite and silicon-based subcells can have good current matching by adjusting the thickness of the interconnection layer and the band gap of PSCs, so that the J_{sc} of tandem cells is considered half of the J_{sc} of silicon-based cell.

So that a value of about 20.0 mA/cm^2 has been taken as the short-circuit current density of the monolithic two-terminal tandem PV device. Nevertheless, in the calculation, we have to take the J_{sc} value of metal halide perovskite cell if the J_{sc} value of perovskite is less than half of bottom cell, owing to the current matching requirement.

3.2 Open-circuit voltage V_{oc}:

Open-circuit voltage V_{oc} of the tandem cells is conceptually the sum of the two subcell's. However, due to the loss of short circuit current density from top perovskite cell shelter, the V_{oc} of silicon-based bottom cell must has a deficit, thus, the total open circuit voltage is calculated as:

$$V_{oc,\ tandem} = V_{oc,\ top} + V_{oc,\ bottom} + \Delta V_{oc} \qquad \text{(eq. 2)}$$

Where $V_{oc,\ top}$ is open-circuit voltage of top cell, $V_{oc,\ bottom}$ is that of bottom cell, while ΔV_{oc} is a deficit arisen from the decrease of short-circuit current density and a recombination cause of electron and hole in the interconnection layers of the both cells. The reasons for ΔV_{oc} mainly come from two aspects：

（i）Deficiency from short-circuit current density: The ΔV_{oc} of the subcells in the tandem is estimated by the logarithmic dependence of ΔV_{oc} on the photocurrent density (Wurfel et al. 2015). The deficit of open-circuit voltage (ΔV_{oc}) about the SQIS device in this part is:

$$\Delta Voc = \frac{k_B T}{e}\left[ln\left(\frac{J_{sc,before} + J_0}{J_{sc,after} + J_0}\right)\right] \qquad \text{(eq. 3)}$$

Where k_B is Boltzmann constant, T is absolute temperature; J_0 is a recombination current density. Since the order of magnitude of J_o in both cells is a few tens of fA/cm^2 at most, and the order of magnitude of J_{sc} in both cells is in the level of mA/cm^2, so that J_o can be ignored. Thus, if $J_{sc,before} = 40.05\ mA/cm^2$, or $J_{sc,after} = 20.00\ mA/cm^2$, it can be derived that the ΔV_{oc} is about 18.05 mV in terms of eq.3. Nevertheless, for upper perovskite cell, the short circuit current density decreases slightly, hence the deficit of open-circuit voltage is negligible.

（ii）Deficit from interconnection layer: The intermediate layer for connecting two subcells inevitably produces a lower carrier recombination rate, resulting in the accumulation of electrons from perovskite cell and holes from silicon-based cell in the intermediate layer (Campbell et al. 1986). It has been estimated for a tandem system that about 20 mV of ΔV_{oc} is lost mainly due to the electrical loss at the recombination layer (Liu et al. 2015). Thus, the total loss of open-circuit voltage ΔV_{oc} is about 38.05 mV, combined with the loss of open-circuit voltage caused by halving the short-circuit current density mentioned above. It is derived that the open-circuit voltage of planar n-i-p perovskite/SQIS tandem cells with SiO_x-TiN_y rear contact can reach about 1.92 V.

3.3 Filled factor pFF

Ideally, pFF is just a function of open circuit voltage. Owing to the fill factor of any solar cell is dependent on the ratio of carrier's transport velocity to recombination velocity, so do the tandem cells. Therefore, the fill factor of the tandem cells should be dominantly determined by the modified SQIS cell, additionally, the following approximate empirical eq.4 could be deployed to estimate the pseudo-fill factor (pFF), because it is only a function of open circuit voltage (V_{oc}) under ideal conditions and without parasitic shunt resistance (Campbell et al. 1986; Meng et al. 2018).

$$\mathrm{pFF} = [\upsilon - \ln(\upsilon + 0.72)]/(\upsilon + 1) \qquad \text{(eq. 4)}$$

Where υ is the normalized open circuit voltage, given by $\upsilon = \frac{\mathrm{q}\,V_{oc}}{nK_BT}$, where q is electron charge, while n is the ideal factor of a diode and in the range of 1-2. Generally, the pFF value is in the range of 75.6 % - 85.1 % for a tandem cells, dependent on the quality of the cells, but in our case, the optimized value of pFF is estimated to be about 81.19 % for the modified SQIS device.

3.4 Power conversion efficiency η

The conversion efficiency of the tandem cells can also be calculated by the equation 5 as

$$\eta = (J_{sc}V_{oc}FF/P_{in}) \times 100\% \qquad \text{(eq. 5)}$$

Thus, the results of J_{sc}, V_{oc}, pFF and efficiency η are summarized in table 2 for the individual and tandem cells.

Tab. 2: The photoelectric parameters acquired by experimental and numerical calculation

Framework of device	V_{oc} (V)	J_{sc} (mA/cm^2)	FF (%)	η (%)
Modified-SQIS	0.710	40.05	81.19	23.08
Planar n-i-p perovskite（E_g=1.74 eV）[28]	1.25	19.00	81.50	19.10
Planar n-i-p perovskite/SQIS with rear SiO_x/TiN_y	1.92	19.00	81.19	29.62

4. Conclusion

In this investigation, we re-design and prepare new monolithic tandem solar cells through a combination of modified SQIS as bottom cell with n-i-p perovskite as top cell, basing on the concept of spectral response and current matching for both subcells. It is found that the modified SQIS is a good candidate as bottom cell for the tandem system, because the enhancement of near-infrared response (EQE) of the ITO/a-SiO_x (In)/n-Si/SiO_x-TiN heterojunction device with double-tunneling features has been verified by a series of experiments and simulations. In particular, both double layer's composite film materials of ITO/a-SiO_x(In) and SiO_x-TiN are most significant for the built-in potential, carrier's selectivity, passivating contact and quantum transport of the asymmetric PV device, in which the microstructure, chemical configuration and passivation behavior of the front a-SiO_x(In) and rear SiO_x on silicon substrate are totally different, because the negative charge contained in a-SiO_x(In) and positive charge in SiO_x for the field passivation effects of hole and electron are their distinct traits, respectively. On the other side, the higher electron concentration (10^{21}-10^{22} /cm^3) in ITO or TiN films obtained by Hall measurements has manifested that both the films are degenerated materials, such as heavy doped semiconductor or quasi-metals, in that the equivalent Fermi level of a-SiO_x (In) or TiN is localized near to the valence- or conduction bands of n-Si, respectively, benefit to the built-in potential and extraction of photon-generated carriers.

Additionally, the change or increment of electron concentration n_e in TiN_x film is ascribed to a small deficit of nitrogen element during reactive magnetron sputtering process by XPS characterization, and an energy band bending from accumulation, flat and reversion near interface of n-Si/SiO_x-TiN has been gained by the calculation of the shift of conduction band edge in terms of the variation of electron concentration n_e of TiN_x by means of AFORS-HET program. It is also found that the increase in photocurrent density is mainly due to

the increase of EQE near-infrared region, while the decrease in dark current is owing to the reduction of carrier's recombination arisen from the valence band offset between n-Si and TiN_x (2.30 eV), furthermore, the change of electronic barrier at the n-Si/SiO_x-TiN interface is controlled by the n_e of TiN films. Thus, SiO_x-TiN back contact to n-Si plays the multi-roles of interface passivation, electron export, and hole blocking, leading to the increases of open-circuit voltage, short-circuit current, fill factor as well as PCE of the modified SQIS device. So that, a boost increase of the PCE has been obtained in the estimation, which is more than 23.0 %. Moreover, a higher prospective conversion efficiency of 29.0 % for the planar n-i-p perovskite/SQIS with SiO_x-TiN tandem cells has been predicted through an available estimation on the maximum values of J_{sc}, V_{oc} and pFF, mentioned in section 3 and table 2, where the photovoltaic parameters of both perovskite and n-Si based devices are taken from reference [28] and optimized SQIS by means of the state of the art fabrication and numerical simulation. The near-infrared response and enhancement of EQE after SiO_x-TiN back contact to Si-based SQIS device is crucial for improving the performance of modified SQIS and tandem cells as well.

Moreover, there are three key points to successfully realize in the monolithic tandem photovoltaic device: first, the rational design and preparation of silicon-based SQIS device; second, the band gap of halogen perovskite is more than 1.74 eV; third, the intermediate electron - hole recombination layer and other auxiliary thin film materials are preferred. Thus, the requirements of the photovoltaic device principle and the goal of low cost and high efficiency can be achieved.

5. Acknowledgements

This work is mainly supported by the National Natural Science Foundation of China (No. 61874070, 61674099 and 61274067) and the R&D Foundation of the SHU-SOENs PV Joint Laboratory (No. SSE0700601).

6. References

Al-Ashouri, A., et al., 2020. Monolithic perovskite/silicon tandem solar cell with > 29% efficiency by enhanced hole extraction. *Science.* 370, 1300.

Campbell, P., Green, M.A., 1986. The limiting efficiency of silicon solar cells under concentrated sunlight. IEEE Transactions on Electron Devices, 33, 234.

Chen, B., et al., 2019. Grain engineering for perovskite/silicon monolithic tandem solar cells with efficiency of 25.4%. *Joule*, *3*, 177.

Dreiner, S., Schürmann, M., Westphal, C., Zacharias, H., 2001. Local Atomic Environment of Si Suboxides at the SiO_2/Si (111) Interface Determined by Angle-Scanned Photoelectron Diffraction. Phys. Rev. Lett. 86, 4068

Du, H. W., et al., 2015. Preparation of ITO/SiOx/n-Si solar cells with non-decline potential field and hole tunneling by magnetron sputtering. Appl. Phys. Lett. 106, 093508.

Eperon, G. E., Hörantner, M. T., Snaith, H. J., 2017. Metal halide perovskite tandem and multiple-junction photovoltaics. Nat. Rev. Chem. 1 (12), 0095.

Gao, M., et al., 2017. An effective passivation and tunneling hybrid a-SiO_x (In) layer in ITO/n-Si heterojunction photovoltaic device. ACS Appl. Mat. Interface 9(20), 17565.

Liu, B.F., et al., 2015. High efficiency triple junction thin film silicon solar cells with optimized electrical structure. Progress in Photovoltaics. 23, 1313.

Liu, Z., et al., 2020. A holistic approach to interface stabilization for efficient perovskite solar modules with over 2,000-hour operational stability. *Nat. Energy* 5, 596.

Jošt, M., et al., 2018. Textured interfaces in monolithic perovskite/silicon tandem solar cells: Advanced light management for improved efficiency and energy yield. *Energy Environ. Sci. 11*, 3511.

Jošt, M., Kegelmann, L., Korte, L., Albrecht, S., 2020. Monolithic Perovskite Tandem Solar Cells: A Review of the Present Status and Advanced Characterization Methods Toward 30% Efficiency, Adv. Energy Mater. 10, 1904102 and references therein.

Jeong, J., et al., 2021a. Pseudo-halide anion engineering for α-$FAPbI_3$ perovskite solar cells. Nature 592, 381.

Jeong, J., et al., 2021b. Efficient perovskite solar cells via improved carrier management. Nature 590, 587.

Kobayashi, A. H. et al., 2010. Nitric acid oxidation of Si (NAOS) method for low temperature fabrication of SiO_2/Si and SiO_2/SiC structures. Appl. Surf. Sci. 256 (19), 5744.

Kim, D. H., et al., 2019. Bimolecular additives improve wide-band-gap perovskites for efficient tandem solar cells with CIGS. *Joule* 3, 1734.

McMeekin, D. P., et al., 2016. A mixed-cation lead mixed-halide perovskite absorber for tandem solar cells. Science 351, 151.

Meng, L., et al., 2018. Organic and solution-processed tandem solar cells with 17.3% efficiency, Science, 361, 1094.

Mazzarella, L., et al., 2019. Infrared Light Management Using a Nanocrystalline Silicon Oxide Interlayer in Monolithic Perovskite/Silicon Heterojunction Tandem Solar Cells with Efficiency above 25%**.** *Adv. Energy Mater. 9*, 1803241.

NREL. *Best Research-Cell Efficiency Chart* https://www.nrel.gov/pv/cell-efficiency.html (accessed 17 March 2021).

Nelson, C. A., Monahan, N. R., Zhu, X.-Y., 2013. Exceeding the Shockley-Queisser limit in solar energy conversion. Energy Environ. Sci. 6 (12), 3508.

Nogay, G., et al., 2019. 25.1%-Efficient Monolithic Perovskite/Silicon Tandem Solar Cell Based on a p-type Monocrystalline Textured Silicon Wafer and High-Temperature Passivating Contacts. *ACS Energy Lett. 4*, 844.

Roß, M., et al., 2021. Co-Evaporated Formamidinium Lead Iodide Based Perovskites with 1000 h Constant Stability for Fully Textured Monolithic Perovskite/Silicon Tandem Solar Cells. Adv. Energy Mater. 11, 2101460.

Shockley, W., Queisser, H. J., 1961. Detailed balance limit of efficiency of p−n junction solar cells. J. Appl. Phys. 32 (3), 510.

Sahli, F., et al., 2018. Fully textured monolithic perovskite/silicon tandem solar cells with 25.2% power conversion efficiency. *Nat. Mater. 17*, 820.

Song, X. M., et al., 2018. Interface Properties of ITO/n-Si Heterojunction Solar Cell: Quantum Tunneling, Passivation and Hole-Selective Contacts. Solar Energy 173, 456.

Tan, H., et al., 2018. Dipolar cations confer defect tolerance in wide-bandgap metal halide perovskites. Nature Communications 9, 3100.

Wurfel, U. D., Spies, N. A., Albrecht, S., 2015. Impact of charge transport on current-voltage characteristics and power-conversion efficiency of organic solar cells. Nat Commun. 6, 6951.

Wan, Y.Z., et al., 2017. Potentiality of delocalized states in indium-involved amorphous silicon oxide. Applied Physics Letters 110, 213902.

Wu, K. J., et al., 2020. Improvement of the performance of ITO/a-SiOx/n-Si device by controllable sputtering power and reducible interface states. Mater. Sci. in Semicon. Processing 105, 104702.

Wang, R., et al., 2021. Prospects for metal halide perovskite-based tandem solar cells Nat. photonics. 15, 411.

Yoshikawa, K., et al., 2017. Silicon heterojunction solar cell with interdigitated back contacts for a photoconversion efficiency over 26%. *Nat. Energy* **2**, 17032.

Yang, Z.B., et al., 2019. Enhancing electron diffusion length in narrow bandgap perovskites for efficient monolithic perovskite tandem solar cells. Nature communications 10, 4498.

Zheng, X. et al., 2020. Managing grains and interfaces via ligand anchoring enables 22.3%-efficiency inverted perovskite solar cells. *Nat. Energy* 5, 131.